Sidelobe Reduction for Limited Diffraction Pulse-Echo Systems

Jian-yu Lu, *Member, IEEE,* and James F. Greenleaf, *Fellow, IEEE*

Abstract—**Conventional focused transducers have a sharp focal spot with low sidelobes but, they have a short depth of field. Commercial medical scanners obtain increased depth of field by combining several images in a montage, each obtained at a different focal depth. Therefore, to get low sidelobes over a large depth of field several transmits must be used, which decreases the frame rate. Limited diffraction beams such as Bessel beams and X waves obtain good resolution over very large depth of field but, they have high sidelobes. We have developed a summation–subtraction method for decreasing the sidelobes. The method requires three transmits, decreasing the frame rate to one third. Although others have tried the same technique, we apply it to limited diffraction beams and obtain an analytic description.**

I. Introduction

LIMITED diffraction beams have been studied recently. These beams have a large depth of field even if they are produced with a finite aperture and energy. The first localized solution to the isotropic/homogeneous scalar wave equation was discovered in electromagnetics by Brittingham in 1983 [1] and was termed focus wave modes. Two years later, in 1985, a new localized solution to the scalar wave equation was developed by Ziolkowski [2]. The new localized solution was used to construct other localized solutions such as the modified power spectrum pulses [3]. Independent of Brittingham and Ziolkowski's works, in 1987, Durnin [4] discovered the first limited diffraction solution to the scalar wave equation and called it "nondiffracting" or "diffraction-free" beams (we use the term "limited diffraction beams" to avoid the controversy of Durnin's original terminologies). Durnin's beams are also called Bessel beams because their lateral profiles are Bessel functions. The Bessel beams were verified with optical experiments [5]–[7]. Hsu *et al.* produced a zeroth-order Bessel beam with a narrow-band ultrasonic transducer [8]. Campbell *et al.* [9] have studied the zeroth-order Bessel beam theoretically and made the same suggestion as we did to produce the Bessel beam with an acoustic annular array [10]. We have produced a broadband zeroth-order Bessel beam with an ultrasonic annular array transducer and applied it to medical imaging, biological tissue characterization, and nondestructive evaluation of materials [10]–[19]. In addition, we have reported new families of limited diffraction solutions of the scalar wave equations [20]–[23]. These solutions are a generalization of the limited diffraction beams known previously in addition to an infinity of new beams such as X waves. The X waves are nonspreading-nondispersive and superluminal, and have an X-like shape in a plane along the propagation axes. We have also generalized the limited diffraction solutions to an n-dimensional scalar wave equation [24]. Recently, a mechanical scanned annular array that can produce either limited diffraction beams or conventional focused beams was built and was applied to real-time *in vitro* and *in vivo* medical imaging [25]. The possibility of steering limited diffraction beams with a two-dimensional array was also studied [26].

Although limited diffraction beams could have many practical applications, sidelobes of these beams are higher than those of conventional focused beams at their focuses. Sidelobes will lower contrast when limited diffraction beams are applied to medical imaging affecting the detection of low scatter objects such as small cysts. In addition, sidelobes increase the effective sampling volume and thus average out spatially distinguished information in tissue characterization. Sidelobes are also a source of multiple scattering that produces artifacts in nondestructive evaluation of materials [13].

In this paper, we report a method for reducing the sidelobes of pulse-echo responses of limited diffraction beams. This method is similar to those used for the ring transducer of Burckhardt *et al.* [27] and the hybrid Axicon of Patterson *et al.* [28]. A theoretical analysis for using a summation-subtraction method to reduce the sidelobes of limited diffraction pulse-echo systems was developed. Simulations with a finite aperture radiator were performed to validate the theory (with a formula developed for calculating pulse-echo responses of any-order limited diffraction beams under the Fresnel approximation [29]). Though the above method can reduce the sidelobes dramatically, it lowers the imaging frame rate to one third because three A-lines obtained at each transducer position are required. The penalty paid on imaging frame rate is similar to that of conventional focused beams, where a montage process is used to increase the depth of field while keeping lower sidelobes. The montage process requires sub-images obtained around separate transmit focuses of the conventional beams, which requires multiple beam transmissions and thus lowers the imaging frame rate.

It is noted that although low sidelobes over a large depth of field can be obtained with conventional focused beams through montaging, drawbacks of these beams remain. First, these beams are still diffracting after the montage process. Images obtained will be sharper near a transducer and gradually

Manuscript received May 15, 1993; revised July 20, 1993; accepted July 28, 1993. This work was supported in part by the National Institutes of Health under Grant CA 43920 and Grant CA 54212.

The authors are with the Biodynamics Research Unit, Department of Physiology and Biophysics, Mayo Clinic and Foundation, Rochester, MN 55905.

IEEE Log Number 9212127.

0885-3010/93$03.00 © 1993 IEEE

blurred in deeper depths since the f-number of the transducer increases with the depth. The depth dependence of image resolution is undesirable if image restoration techniques such as deconvolution are to be used for further improvement of image quality. Second, the focal lengths of conventional beams change with speeds of sound. Thus, either the transducer or its associated electronics need to be changed to maintain given focal lengths for nondestructive evaluation of materials of different speeds of sound. In addition, the montage process is usually more complex than doing A-line summation and subtraction in a machine.

In the next section, we will give a theoretical background for certain families of limited diffraction beams. The equations given in that section will be used for developing the sidelobe reduction method that follows. In Section III, a theoretical analysis of the sidelobe reduction method for pulse-echo systems using limited diffraction beams is reported. Simulations of pulse-echo images obtained from a finite aperture radiator are given in Section IV. A discussion and conclusion are presented in Sections V and VI, respectively. A formula for simulating pulse-echo responses of limited diffraction beams of any order, under the Fresnel approximation is given in Appendix B.

II. Theory of Limited Diffraction Beams

In the following, we will derive new equations of Bessel beams [4] and X waves [20], [21] generalized for any order, m. These equations represent non-rotating beams in a transverse plane and are different from what we derived before [20], [21]. They are the bases for the sidelobe reduction method developed in the next section.

A. One Family of Solutions to the N-dimensional Scalar Wave Equation

Many physical phenomena in acoustics, electromagnetics, and optics are governed by wave equations. An n-dimensional scalar wave equation for source-free, loss-less, and isotropic/homogeneous media is given by [30]

$$\left[\sum_{j=1}^{n}\frac{\partial^2}{\partial x_j^2}-\frac{1}{c^2}\frac{\partial^2}{\partial t^2}\right]\Phi=0 \tag{1}$$

where x_j, $(j=1,2,\cdots,n)$, represent rectangular coordinates in an n-dimensional space, t is time, n is an integer, c is a constant and represents the speed of wave, and $\Phi=\Phi(x_1,x_2,\cdots,x_n;t)$ is an n-dimensional complex wave field. In the physical world, only the real or imaginary part of a complex wave is produced.

Equation (1) has numerous solutions. One family of solutions is given by [24]

$$\Phi(x_1,x_2,\cdots,x_n;t)=f(s) \tag{2}$$

where

$$s=\sum_{j=1}^{n-1}D_jx_j+D_n(x_n-c_1t),\qquad n\geq 1 \tag{3}$$

and where

$$c_1=\pm c\sqrt{1+\sum_{j=1}^{n-1}D_j^2/D_n^2},\qquad n\geq 1 \tag{4}$$

and where D_j are any complex coefficients, and $f(s)$ is any well-behaved complex function of s. We assume that $n\neq 0$, otherwise, $f(s)$ is only a function of time and represents a vibration.

B. Limited Diffraction Solutions

If c_1 in (3) is real, $f(s)$ represents a limited diffraction wave propagating along axis, x_n, at the phase velocity of c_1, in an n-dimensional space [24]. By limited diffraction we mean that travelling with the wave, one sees a complex wave pattern that does not change with time. This means that if $x_n-c_1t=$ constant, $f(s)$ is not a function of time, t. In the following we chose the "+" sign in (4) that represents a forward going wave. Results will be similar if a backward going wave is studied.

Numerous solutions can be constructed from the family of solutions, $f(s)$, by a linear superposition [20]. New solutions that represent non-rotating Bessel beams and X waves are two examples.

C. Non-Rotating Bessel Beams

Letting $n=3$, $x_1=x$, $x_2=y$, $x_3=z$, $D_1=i\alpha\cos\theta$, $D_2=i\alpha\sin\theta$, $D_3=i\beta$, $f(s)=e^s$, where α is a constant, $\beta=\omega/c_1=\sqrt{(\omega/c)^2-\alpha^2}>0$ is real, ω is angular frequency, θ is a free parameter, and integrating $(1/2\pi)i^{-m}\cos m(\theta-\phi_0)f(s)$ over θ from $-\pi$ to π, one obtains an mth-order non-rotating Bessel beam

$$\Phi_{J_m}(s)=J_m(\alpha r)\cos m(\phi-\phi_0)e^{i(\beta z-\omega t)},\quad m=0,1,2,\cdots \tag{5}$$

where m is an integer, J_m is an mth-order Bessel function of the first kind, $r=\sqrt{x^2+y^2}$ is a radial distance, $\phi=\tan^{-1}(y/x)$ is an azimuthal angle, and ϕ_0 is an initial azimuthal angle (polarization) of the beams at the plane, $z=0$. The non-rotating Bessel beams given by (5) are also exact solutions to the wave equation (1) (see Appendix A). They are different from the former Bessel beams by replacing $e^{im\phi}$ with $\cos m(\phi-\phi_0)$.

D. Non-Rotating X Waves

Non-rotating X waves can also be obtained by choosing different coefficients in (3) and integrating over different paramters. Letting $n=3$, $x_1=x$, $x_2=y$, $x_3=z$, $D_1=ik\sin\zeta\cos\theta$, $D_2=ik\sin\zeta\sin\theta$, $D_3=ik\cos\zeta$, $f(s)=e^s$, where $k=\omega/c$ is the wavenumber, ζ is a free parameter, and integrating $(1/2\pi)i^{-m}\cos m(\theta-\phi_0)B(k)e^{-a_0k}f(s)$ over θ from $-\pi$ to π and over k from 0 to ∞ [20], one obtains an mth-order non-rotating X wave

$$\Phi_{X_m}=\cos m(\phi-\phi_0)\int_0^\infty B(k)J_m(kr\sin\zeta)\cdot e^{-k[a_0-i\cos\zeta(z-c_1t)]}dk,\qquad m=0,1,2,\cdots \tag{6}$$

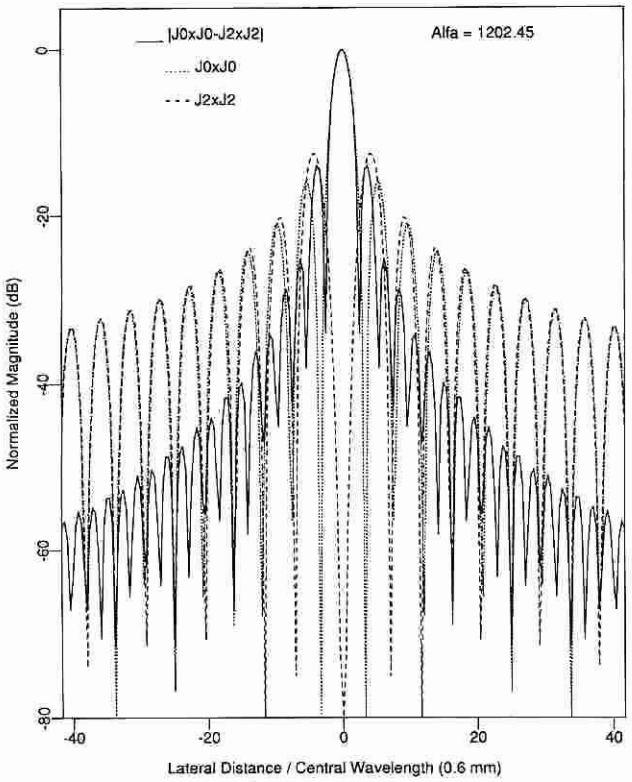

Fig. 1. Squares of the zeroth-order (dotted line) and second-order (dashed line) Bessel functions of the first kind and the absolute value of their subtraction (full line).

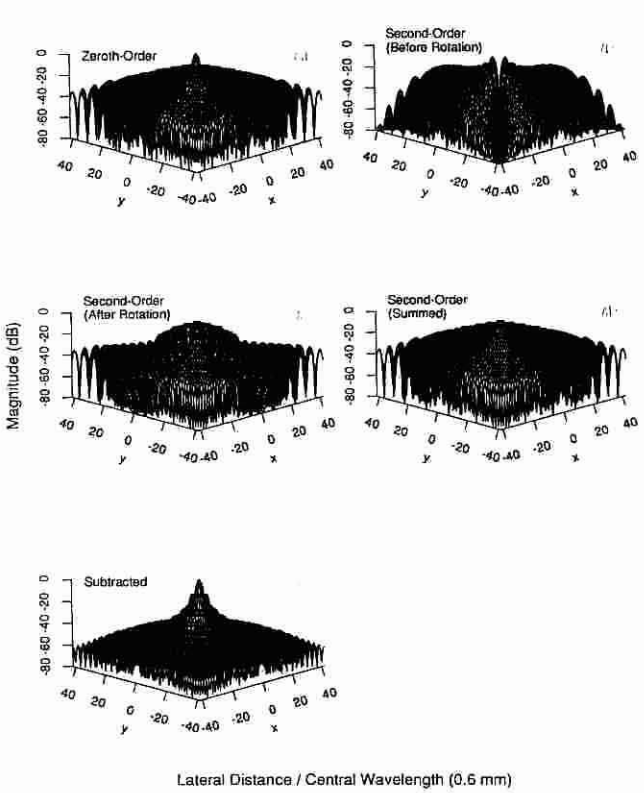

Fig. 2. Point spread functions of a Bessel beam pulse-echo system in a transverse plane. (a) zeroth-order Bessel pulse-echo system, (b) second-order Bessel pulse-echo system with $\phi_0 = 0$, (c) second-order Bessel pulse-echo system with $\phi_0 = \pi/4$, (d) summation of the two point spread functions of the second-order Bessel pulse-echo systems, and (e) absolute value of subtraction between Panels (d) and (a). Note that Panel (d) does not have a mainlobe.

where $B(k)$ is the transmitting or receiving transfer function of a transducer, a_0 is the constant that determines the fall off speed of the high frequency component of the X waves, and $c_1 = c/\cos\zeta$ is the phase velocity. Equation (6) is also an exact solution to the wave equation (1). Compare (5) to (6), it is seen that X waves have a constant phase velocity for all frequency components. This means that X waves are nondispersive in an isotropic/homogeneous medium as will be seen from Fig. 6 in Section IV.

We will use (5) and (6) to show that the sidelobes of limited diffraction beams can be reduced using a summation–subtraction method. The sidelobe reduction method works in principle on systems that transmit limited diffraction beams and receive echoes with the same limited diffraction responses, i.e., on limited diffraction pulse-echo systems.

III. Method for Sidelobe Reduction

We will first derive the signals returned from a point scatterer and received with a limited diffraction pulse-echo system. We then show the sidelobe reduction of these systems with a summation-subtraction method.

A broadband Bessel beam is given by [9], [11]

$$\Phi_{J_m} = \frac{1}{2\pi}\int_{-\infty}^{\infty} d\omega[2\pi T(\omega)J_m(\alpha r)\cos m(\phi-\phi_0)e^{i\beta z}]e^{-i\omega t} = 2\pi J_m(\alpha r)\cos m(\phi-\phi_0)\mathcal{F}^{-1}\{T(\omega)e^{i\beta z}\},$$

$$m = 0, 1, 2, \cdots \tag{7}$$

where $T(\omega)$ is the transmit transfer function of a transducer (Fourier transform of an impulse response) and where $\mathcal{F}^{-1}$ represents an inverse Fourier transform that is defined as

$$f(t) = \mathcal{F}^{-1}\{F(\omega)\} = \frac{1}{2\pi}\int_{-\infty}^{\infty} d\omega F(\omega)e^{-i\omega t} \tag{8}$$

and where $f(t)$ and $F(\omega)$ are a Fourier transform pair. Equation (7) is still an exact solution of (1) since it is simply a linear superposition of (5) over the free parameter, ω. Assuming that the receive transfer function of the transducer is the same as that of the transmit, from the reciprocal principle, one obtains signals returned from a point scatterer located at $\vec{r} = (r, \phi, z)$

$$e_{J_m}(\vec{r}, t) = 4\pi^2 J_m^2(\alpha r)\cos^2 m(\phi-\phi_0)\mathcal{F}^{-1}\{T^2(\omega)e^{i2\beta z}\}, \quad m = 0, 1, 2, \cdots. \tag{9}$$

If point scatterers are distributed in the half space, $z \geq 0$, and multiple scattering among the scatterers is negligible, the

electrical signals from the transducer are given by

$$e_{J_m} = 4\pi^2 \int_{-\infty}^{\infty} r dr \int_{-\pi}^{\pi} d\phi \int_0^{\infty} dz \cdot [A(r,\phi,z) J_m^2(\alpha r)\cos^2 m(\phi-\phi_0)] \cdot \mathcal{F}^{-1}\{T^2(\omega)e^{i2\beta z}\}], \qquad m = 0,1,2,\cdots \quad (10)$$

where $A(r,\phi,z)$ represents the reflection coefficient of the scatterers.

From the properties of the Bessel functions [31], it is noted that for $r = 0$, $J_0^2(\alpha r)$ and $J_2^2(\alpha r)$ are one and zero, respectively, and both $J_0^2(\alpha r)$ and $J_2^2(\alpha r) \to (2/\pi\alpha r)\cos^2(\alpha r - (\pi/4))$ as $\alpha r \gg 1$. $J_0^2(\alpha r)$ and $J_2^2(\alpha r)$ are also very close to each other for other values of αr except for the first few sidelobes. Therefore, subtracting $J_2^2(\alpha r)$ from $J_0^2(\alpha r)$ could result in a significant sidelobe reduction (see Fig. 1). To perform the subtraction, the ϕ dependent term associated with the higher order Bessel beams ($m \geq 1$) in (10) must be removed. This can be done by adding two RF A-lines obtained with the transducer rotated one quarter period ($\pi/(2m)$ for $m = 2$) relative to each other (note that $\cos^2 m\phi + \cos^2 m(\phi - \pi/(2m)) \equiv 1$). Therefore, sidelobes could be reduced by first summing two second-order RF A-lines and then subtracting the result from a zeroth-order A-line

$$e_{J_0}(t) - [e_{J_2}(t)|_{\phi_0=0} + e_{J_2}(t)|_{\phi_0=\pi/4}] = 4\pi^2 \int_{-\infty}^{\infty} r dr \int_{-\pi}^{\pi} d\phi \int_0^{\infty} dz A(r,\phi,z) \cdot [J_0^2(\alpha r) - J_2^2(\alpha r)]\mathcal{F}^{-1}\{T^2(\omega)e^{i2\beta z}\}, \quad (11)$$

For larger r, $|J_0^2(\alpha r) - J_2^2(\alpha r)| \approx 0$ in (11), and thus the scatterers in those areas have little contribution to the combined echo signals. This greatly reduces the sidelobes. A pulse-echo image of reduced sidelobes can be formed from the above A-lines by scanning the transducer. In Fig. 2, a sidelobe reduction process is demonstrated with the point spread functions of a Bessel pulse-echo system.

For X waves, a similar summation–subtraction formula can be obtained from (6)

$$e_{X_0}(t) - [e_{X_2}(t)|_{\phi_0=0} + e_{X_2}(t)|_{\phi_0=\pi/4}] = \frac{4\pi^2}{c^2} \int_{-\infty}^{\infty} r dr \int_{-\pi}^{\pi} d\phi \int_0^{\infty} dz A(r,\phi,z)\mathcal{F}^{-1} \cdot \left\{ \left[J_0^2\left(\frac{\omega}{c} r\sin\zeta\right) - J_2^2\left(\frac{\omega}{c} r\sin\zeta\right)\right] \cdot B^2\left(\frac{\omega}{c}\right) H^2\left(\frac{\omega}{c}\right) e^{-i2(\omega/c)a_0} e^{i2(\omega/c)z\cos\zeta} \right\} \quad (12)$$

where

$$H\left(\frac{\omega}{c}\right) = \begin{cases} 1, & \omega \geq 0 \\ 0, & \omega < 0 \end{cases}$$

is the Heaviside step function [32]. The mechanism of the sidelobe reduction with (12) is the same as that with (11) and is also illustrated by Figs. 1 and 2.

GEOMETRY OF BEAD PHANTOM

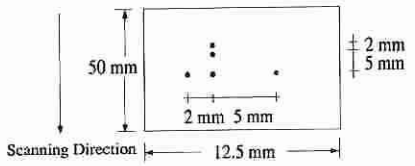

Fig. 3. An object consisting of 5 point scatterers in the plane, $\phi = 0$ (or $y_0 = 0$), for simulation of pulse-echo images (modified with permission from [11]).

IV. Computer Simulations and Results

The above theory for the sidelobe reduction of the limited diffraction pulse-echo systems can be tested with computer simulations. In Appendix B we derive the following formula for calculating the pulse-echo responses of Bessel beams or X waves of any order from a point scatterer located at $\vec{r}_0 = (x_0, 0, z)$ (point spread function) under the Fresnel approximation [29];

$$e(\vec{r}_0, t) = \cos^2 m\phi_0 \mathcal{F}^{-1}\{\tilde{\Phi}_A^2(\vec{r}_0,\omega)\} \quad (13)$$

where

$$\tilde{\Phi}_A(\vec{r}_0,\omega) = \left(\frac{2\pi}{i\lambda} + \frac{1}{\sqrt{x_0^2+z^2}}\right) \frac{z e^{i(k\sqrt{x_0^2+z^2}+m\pi/2)}}{(x_0^2+z^2)} \cdot \int_0^a \tilde{\Phi}_1(r_1,\omega) e^{ik(r_1^2/2\sqrt{x_0^2+z^2})} \cdot J_m\left(-k\frac{x_0 r_1}{\sqrt{x_0^2+z^2}}\right) r_1 dr_1 \quad (14)$$

and where

$$\tilde{\Phi}_1(r_1,\omega) = 2\pi T(\omega) J_m(\alpha r_1) \quad (15)$$

for Bessel beams and

$$\tilde{\Phi}_1(r_1,\omega) = \frac{2\pi}{c} B(k) J_m(k r_1 \sin\zeta) H(k) e^{-a_0 k} \quad (16)$$

for X waves.

The following results demonstrate the reduction of sidelobes of limited diffraction pulse-echo systems by subtracting the pulse-echo A-lines calculated from (13).

An object consisting of five point scatterers [11] located in the plane $y_0 = 0$ (see Fig. 11 in Appendix B) is shown in Fig. 3. The transducer is assumed to scan in the transverse direction along the axis, x_0, and is aligned for $\phi_0 = 0$ (or $\cos^2 m\phi_0 = 1$ in (13)).

Envelopes of simulated pulse-echo images with the zeroth-order and second-order Bessel beams in both transmit and receive, and their difference images (obtained by subtracting RF signals and then taking the envelopes) are shown in Fig. 4. The transducer is assumed to have a diameter of 50 mm with a central frequency of 2.5 MHz. The scaling parameter of the Bessel beams is $\alpha = 1202.45\,\mathrm{m}^{-1}$, and the depth of field is about 216 mm. The Fourier transform of the impulse

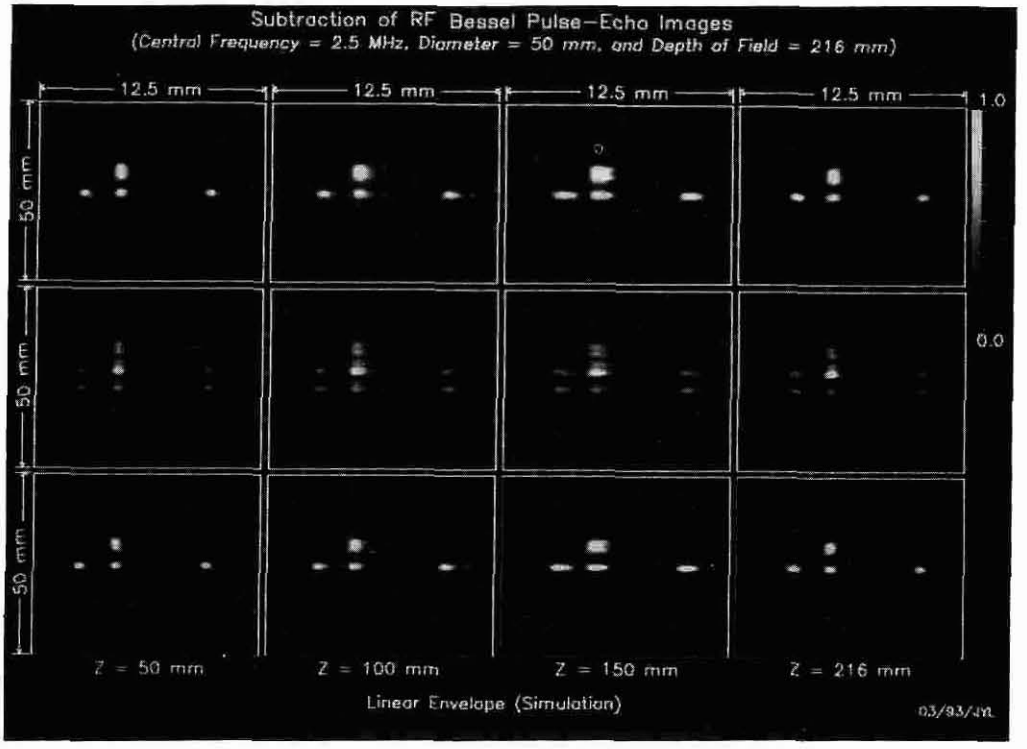

Fig. 4. Envelopes of the simulated pulse-echo images of the object in Fig. 3 with the Bessel beams in both transmit and receive at four axial distances: 50 mm (first column), 100 mm (second column), 150 mm (third column), and 216 mm (fourth column). The images in the first and second rows are obtained with the zeroth- and second-order Bessel beams, respectively. The images in the third row are results after the subtraction of the RF images corresponding to the second row from the RF images corresponding to the first row. The Grey scale of the images represents the envelope of the pulses in a linear scale.

response of the transducer is assumed to be a Blackman window function [33] peaked at 2.5 MHz (see $T(\omega)$ in (15)) and a δ-pulse is used to excite the transducer. The aperture of the transducer is weighted with the exact Bessel functions (15), as well as the angular-dependent term $\cos m(\phi_1 - \phi_0)$ in (5), where ϕ_1 is the angular position of a point on the transducer surface. Fig. 5 shows the lateral line plots of the rightmost point scatterer (Fig. 3) of the images in Fig. 4. To show the sidelobes, the vertical scale of the plots represents the maximum of the envelope of each A-line produced by the rightmost scatterer (since there are other point scatters on the left, only the right portion of the A-lines that begins from a vertical bar that passes through the peak of the image of the rightmost scatter is taken into account, see Fig. 4). Both RF and envelope subtractions are presented in Fig. 5. The envelope subtraction means subtraction between envelope detected images. It results in lower sidelobes but it may have limitations that will be discussed in the next section.

Images in Fig. 6 are obtained with the X waves. The transducer and scanning format for obtaining Fig. 6 are the same as those for Fig. 4. Exact X wave aperture weightings (16), as well as the angular-dependent term $\cos m(\phi_1 - \phi_0)$ in (6) are used. The parameters in (16) are assumed to be as follows: $B(\omega/c) = T(\omega)$ is a Blackman window function, $a_0 = 0.05$ mm, $\zeta = 6.6°$, and the depth of field of the X waves [20] is about 216 mm. The lateral line plots of the envelope through the rightmost point scatterer of Fig. 3 are shown in Fig. 7 for X waves.

V. Discussion

A. Resolution and Depth of Field

The resolution of the pulse-echo images obtained with the zeroth-order limited diffraction beams is about the same as that of the images obtained after the subtraction of the second-order beams. The depth of field of the beams before and after the sidelobe reduction is also the same (see Figs. 4 and 6). This can be expected since both the zeroth- and second-order limited diffraction beams have about the same depth of field for a given transducer size. The second-order limited diffraction beams do not have a mainlobe and their sidelobes are close in amplitude to those of the zeroth-order beams. Therefore, the mainlobe of the zeroth-order beams remains about the same before and after the sidelobe reduction, see Fig. 1.

B. Sidelobes

The sidelobes of the limited diffraction pulse-echo systems are reduced dramatically after the summation–subtraction of A-lines (see Figs. 5 and 7). Higher order limited diffraction beams having sidelobes closest to those of the zeroth-order beams must be chosen for the best results. In this paper we chose the second-order beams. Subtraction, in principle, should be done with RF signals. However, subtraction with envelope signals has shown a further reduction of the sidelobes (see Figs. 5 and 7). The reasons may be that the envelope signals

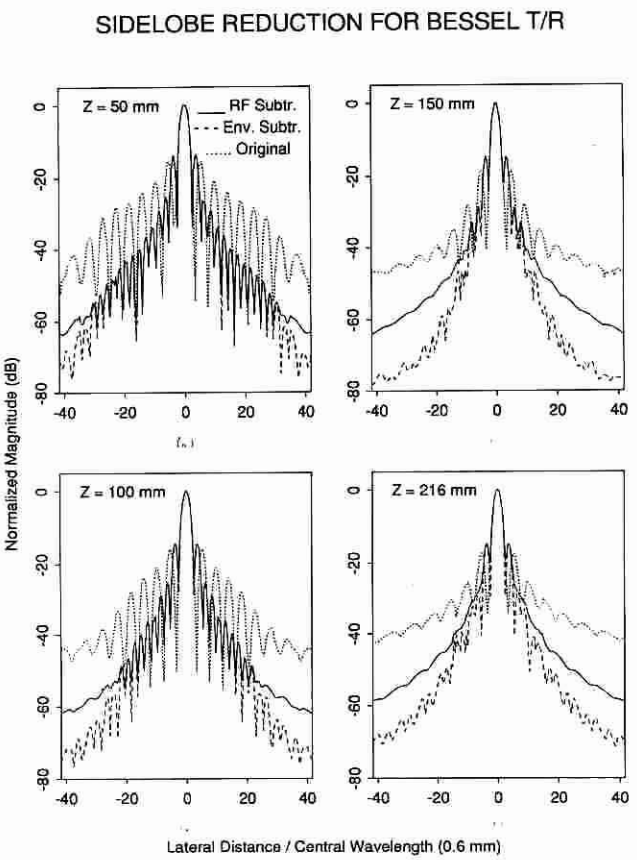

Fig. 5. Lateral line plots of the Bessel beam pulse-echo images of the rightmost point scatterer in Fig. 3. The vertical axes of the plots represent the maximum of the envelope of each A-line of the rightmost point scatterer. The dotted lines represent the plots before sidelobe reduction. The full and dashed lines correspond to the images after RF and envelope subtractions, respectively. The plots are obtained at four axial distances corresponding to the images in Fig. 4: (a) 50 mm, (b) 100 mm, (c) 150 mm, and (d) 216 mm. The lateral axes are normalized to the central wavelength of the beam (0.6 mm).

do not vary as fast with time as the RF signals (see Fig. 8), and in the simulation, there are only a few scatterers that are distributed in one plane (see Fig. 3). Since envelope detection involves nonlinear processes and removes phase information, subtraction with envelopes could not effectively reduce the sidelobe if there are many scatterers distributed randomly in a three-dimensional space. In addition, the summation of signals from the two rotated higher-order limited diffraction beams should also be done with RF signals to remove the angular-dependent terms (see (10)).

Comparing Figs. 5 and 7 to Fig. 1 (see the RF subtractions), it is seen that the simulations are predicted by the theory ((11) and (12)).

C. Object Motion

Apparently, the sidelobe reduction method will be sensitive to the motion of the objects imaged since it involves RF summation and subtraction. However, if the time between adjacent A-lines to be summed and then subtracted is short enough, motion artifacts might be negligible. For still objects, the summation and subtraction can be done either A-line by A-line or after a whole pulse-echo image is obtained.

D. Stepwise Aperture Weighting

In practice, an exact aperture weighting given by, $\tilde{\Phi}(\vec{r}_1, \omega)$, in (B1) is usually hard to apply as seen from (15) and (16), as well as the angular-dependent term $\cos m(\phi_1 - \phi_0)$ in (5) and (6). Therefore, stepwise aperture weightings in both radial and angular directions may have to be used [11], [21]. The stepwise approximation will alter both the radial and angular dependence of the beams and will have influence on the sidelobe reduction. However, as the steps become finer and the weightings approach the exact ones, the influence would be smaller [34]. Practical imaging systems applying the summation–subtraction method for limited diffraction beams will have to compromise between the efficacy of the sidelobe reduction and the system complexity. A detailed study of the compromise is found in [34].

E. Phase Aberration

In biomedical imaging, phase aberration could be strong in some cases such as breast imaging if the size of a transducer is large [35]. Distortion of beams caused by the phase aberration could alter limited diffraction beams from their theoretical descriptions and, thus, diminish the sidelobe reduction.

F. Edge Waves

Although sidelobes of limited diffraction beams can be reduced by the summation-subtraction method, edge waves are not reduced. However, the sidelobes of the edge waves are also reduced (this can be seen by doing a log compression on the linear gray scale of the images in Figs. 4 and 6).

Axial pulse-echo responses of both limited diffraction beams and conventional beams with a point scatterer located on the propagation axis are shown in Fig. 9. It is seen that edge waves exist for all beams except for a focused beam at the focus. Since the pulse-echo responses of the higher-order limited diffraction beams are zero for a scatterer located on the wave axis, the edge waves of the limited diffraction beams shown in Fig. 9 are the same before and after the sidelobe reduction.

The amplitude of the edge waves in Fig. 9 is smaller than that of the main pulses. The edge waves will be smaller if $z/D \ll 1$, where z and D are the axial distance and the diameter of a transducer. Therefore, the total energy of the edge waves would be much smaller than that of the main pulses. Despite the small total energy, edge waves could be a source of artifacts in imaging producing ghost objects or lower contrast of small cysts.

The number of edge waves of X waves is larger than that of other beams (see Fig. 9(a)). This is because the X waves are composed of two back-to-back cones that have more edges. One way to reduce the edge waves is to apodize the edge of the transducer aperture [20]. However, this will reduce the depth of field of the limited diffraction beams and weaken their depth-independent lateral beam properties.

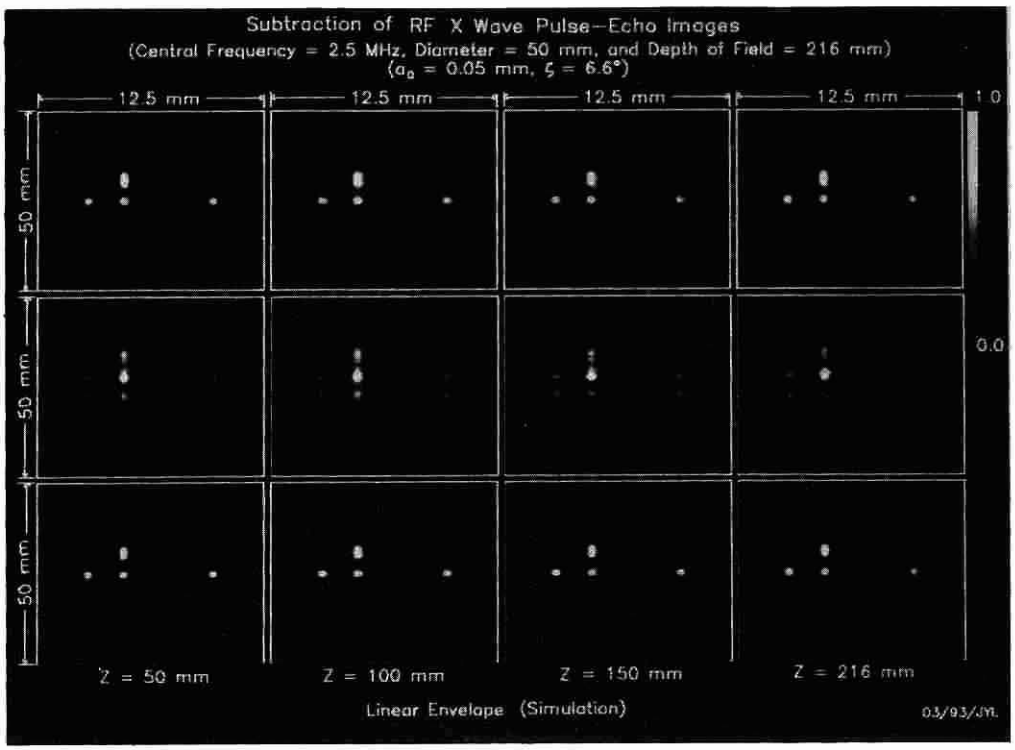

Fig. 6. Envelopes of the simulated X wave pulse-echo images of the object in Fig. 3 at four axial distances: 50 mm (first column), 100 mm (second column), 150 mm (third column), and 216 mm (fourth column) in the same format as that of Fig. 4.

G. Frame Rate

Because three A-lines are needed for the summation-subtraction method to reduce sidelobes of limited diffraction pulse-echo systems at each transducer position, the imaging frame rate will be reduced to 1/3. Use of additional higher order limited diffraction beams could reduce further the sidelobes but lower further the imaging frame rate [27], [36]. The price paid for the sidelobe reduction of the limited diffraction pulse-echo systems is similar to that paid for increasing the depth of field of conventional focused beams that have low sidelobes only at their focuses. The depth of field of the conventional beams is increased by montaging images cut around several focal lengths, each produced by a separate transmit also reducing the imaging frame rate.

Although sidelobes are reduced or depth of field is increased at the expense of imaging frame rate, limited diffraction pulse-echo systems have the following advantages: First, the nonspreading property of limited diffraction beams is preserved after the sidelobe reduction. The limited diffraction pulse-echo systems will have a depth-independent lateral point spread function. In addition, the point spread function is nondispersive for X waves. This means that th eX wave pulse-echo imaging system has also a depth-independent axial resolution (see Fig. 6). With depth-independent point spread function, restoration of images throughout the depth of field could be simplified if the objects imaged do not have strong phase aberration and multiple scattering. Second, the main beamwidth (or focusing property) of the sidelobe-reduced limited diffraction beams will not depend on speed of sound of the materials imaged [9], [13] although the depth of field of the beams may be changed. This is convenient for nondestructive evaluation of materials of different speeds of sound with the same imaging system. Third, the summation and subtraction of A-lines could be simpler to do electronically compared to

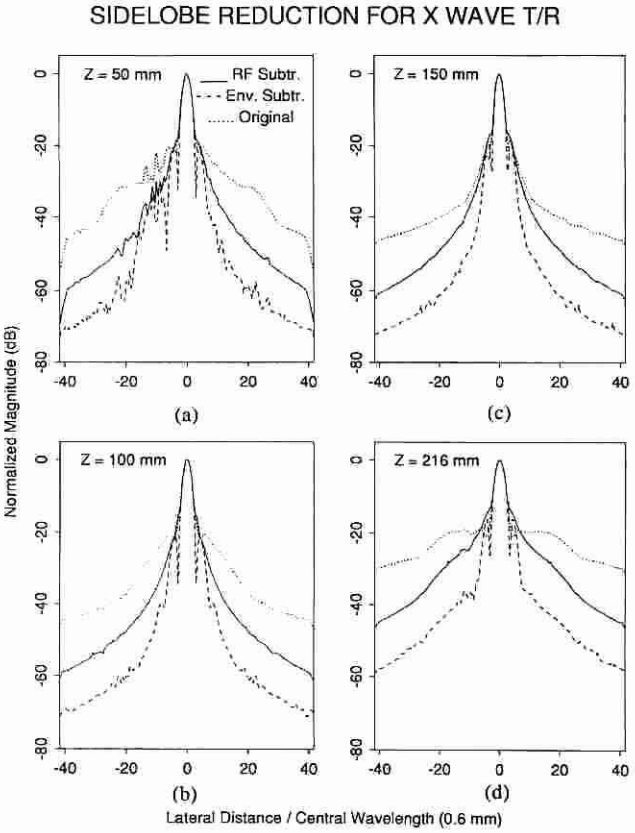

Fig. 7. Lateral line plots of the$X$wave pulse-echo images of the rightmost point scatterer in Fig. 3 shown in the same format as that of Fig. 5.

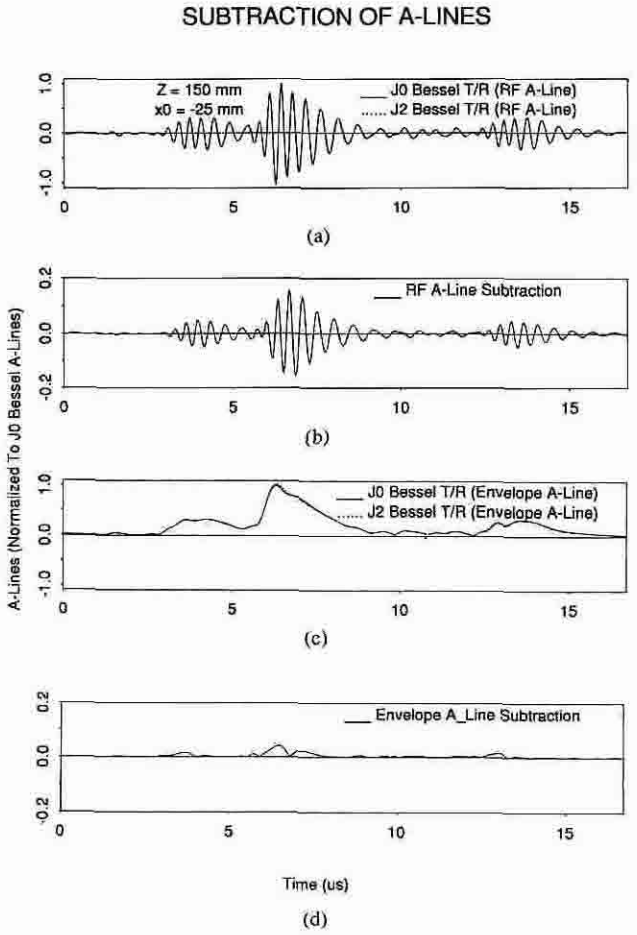

Fig. 8. Subtraction between RF A-lines and between envelope A-lines. These A-lines are obtained from Fig. 4 where the Bessel beams are used in both transmit and receive. The axial distance for these A-lines is 150 mm away from the surface of the transducer and the lateral distance is -25 mm (first lines on the top of the corresponding images). (a) Two RF A-lines obtained with the zeroth- (full line) and second-order (dotted line) Bessel beams, (b) subtraction of the two RF A-lines, (c) the envelopes of the RF A-lines in Panel (a), and (d) subtraction of the envelope A-lines. After removing the carrier frequency, the sidelobes are reduced further after the subtraction. Note that the vertical scales are different for A-lines before and after the subtraction.

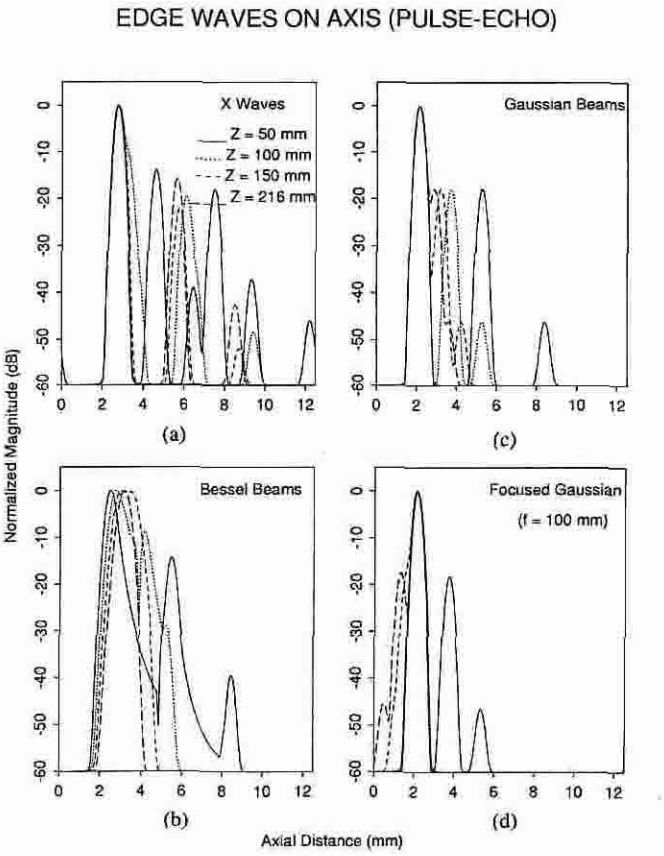

Fig. 9. Axial pulse-echo responses (normalized to their maxima) showing edge waves of (a) X wave, (b) Bessel beam, (c) unfocused Gaussian beam, and (d) focused Gaussian beam ($f = 100$ mm), with a point scatterer located on the wave axis at four distances: 50 mm (full lines), 100 mm (dotted lines), 150 mm (dashed lines), and 216 mm (long dashed lines). The parameters of the X wave and Bessel beam are given in Section III. The Gaussian beams have a full width at half maximum (FWHM) of 25 mm that is the radius of the transducer. Edge waves exist for all beams except focused beams at their focuses. The axial distance is calculated by assuming the speed of sound $c = 1.5$ mm/μs.

the montage process although both methods would be subject to motion artifacts. After increasing the depth of field by the montage process, conventional focused beams are still diffracting because the size of the focal spot increases with depth dramatically as the f-number increases. In addition, focal lengths of focused beams change with the speed of sound of the materials imaged.

H. Receive with Conventional Focused Beam

Limited diffraction beams have a large depth of field but have higher sidelobes than conventional focused beams at their focuses. Therefore, pulse-echo systems that transmit a limited diffraction beam and receive with a conventional focused receiver may combine the advantages of both beams. For this "hybrid" system, sidelobe reduction with the summation-subtraction method is seen in Fig. 10. However, the sidelobe reduction may not be as great if point scatterers are randomly distributed in multiple azimuthal angles because the angular-dependent terms of these hybrid systems may not be removed (recall that in the limited diffraction pulse-echo systems, $\cos^2 m\phi + \cos^2 m(\phi - \pi/(2m)) \equiv 1$, see (10) and (11)).

I. Previous Work

Similar methods have been used for a ring transducer [27] and a hybrid Axicon system [28] to reduce the sidelobes. For the ring transducer, a different approach was used which employed a progressive (rotating) phase term, $e^{i(m(\phi-\phi_0)-\omega t)}$, (instead of $\cos m(\phi - \phi_0)e^{-\omega t}$ as in (5) and (6)) in transmission, and another term of opposite phase, $e^{i(-m(\phi-\phi_0)-\omega t)}$, in reception to cancel each other. Since the exponential phase terms are realized by delaying signals around the ring, the imaging system must be coherent and is not good for broadband applications. Moreover, the Bessel lateral field distributions that are required for the sidelobe reduction can only be produced in the far field of the ring (the Fraunhofer region [29] where the pressure field is proportional to the Fourier transform of the transducer aperture). Therefore, sidelobes can only be reduced in the far field. The far field application of

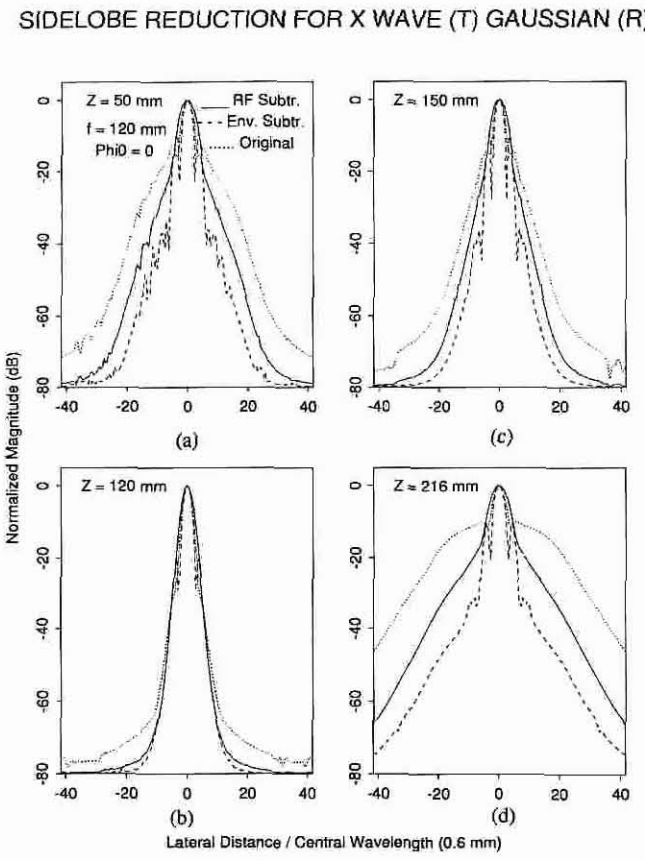

Fig. 10. Lateral line plots of the "hybrid" pulse-echo images of the rightmost point scatterer in Fig. 3, where an X wave is used in transmit and a conventional focused Gaussian beam in receive. The Gaussian beam has a full width at half maximum (FWHM) of 25 mm at the transducer surface and a focal length of 120 mm. The plots are obtained at four axial distances: (a) 50 mm, (b) 120 mm, (c) 150 mm, and (4) 216 mm. The vertical axes of the plots represent the maximum of the envelope of each A-line of the rightmost point scatterer. The dotted lines represent the plots before the sidelobe reduction. The full and dashed lines correspond to sidelobe-reduced images obtained from subtraction with RF and envelope signals, respectively. The lateral axes are normalized to the central wavelength of the beams (0.6 mm). The reduction of sidelobes of this "hybrid" pulse-echo system will be diminished if scatterers are randomly distributed around the beam center because the angular-dependent terms of the system may not be removed.

the ring transducer may lower lateral resolution because the width of the mainlobe of the zeroth-order Bessel function is a linear function of the distance to the surface of the transducer (for limited diffraction beams, the width of the mainlobe is constant in their large depth of field). To increase the lateral resolution, a big ring transducer must be used and this could cause severe phase aberration problems in medical imaging [35] (in [27], a 100-mm diameter ring was used and objects imaged were placed between 200 and 400 mm away from the transducer to avoid the near field and the loss of the lateral resolution). In addition, energy efficiency of a ring transducer is poor since the radiating area of the transducer is small.

For the hybrid Axicon system where an Axicon is used to transmit and a focused annular array is used to receive, no sidelobe reduction was reported when the system was applied to imaging of biological soft tissues [28]. The reasons perhaps are the following: First, this system is similar to that which transmits with a limited diffraction beam and receives with a focused beam as discussed above. Therefore, the efficacy of the summation-subtraction method for sidelobe reduction is diminished when objects imaged are made of random scatterers such as biological soft tissues (recall that $\cos^2 m\phi + \cos^2 m(\phi - \pi/(2m)) \equiv 1$ is only for systems that use limited diffraction beams in both transmit and receive). Second, demodulated images [28] (or envelope) instead of RF images were used. No sidelobe reduction will be obtained this way even if the Axicon had been used in both transmit and receive. In addition, the pressure field distribution of an Axicon in its focal zone is only approximately proportional to the Bessel functions when excited with a CW signal [37]. Analytic expressions similar to (5) and (6) of the Bessel beams and X waves are difficult to obtain for the Axicon. The complexity of the pressure field distribution of the Axicon might reduce the efficacy of the summation–subtraction method for its sidelobe reduction.

J. Applications

The summation–subtraction method for sidelobe reduction of limited diffraction pulse-echo systems might have application in medical imaging. It might increase contrast while keeping the high resolution, large depth of field, and depth-independent point spread functions of the limited diffraction pulse-echo systems. The summation-subtraction method could also be applied to biological tissue characterization, where thinner beams (smaller sidelobes) with no beam diffraction are desirable. The method could also reduce multiple scattering due to sidelobes in nondestructive evaluation, while keeping depth-independent resolution (point spread function) and material-independent focusing properties. In addition, limited diffraction beams with lower sidelobes might have applications in other wave-related areas such as electromagnectics [1]–[3] and optics [4].

VI. Conclusion

A summation–subtraction method for reducing sidelobes of limited diffraction beams is described. This method was derived theoretically and verified with computer simulations for a finite aperture transducer. The results are very encouraging. Around 20 dB of sidelobe reduction is obtained for pulse-echo systems at a lateral distance of about 40 wavelengths. The reduction of sidelobes are increased monotonically with lateral distance. This method could have applications to medical imaging, tissue characterization, nondestructive evaluation of materials, as well as other wave-related areas such as electromagnetics and optics, if movement of objects studied is negligible during the period required for acquisition of three A-lines.

VII. Appendix A

We will verify that (see (5))

$$\Phi_{J_m}(s) = J_m(\alpha r)\cos m(\phi - \phi_0)e^{i(\beta z - \omega t)}, \quad m = 0, 1, 2, \cdots \tag{A1}$$

is an exact solution to the three-dimensional source-free, loss-less, and isotropic/homogeneous scalar wave equation in

cylindrical coordinates [20]

$$\left[\frac{1}{r}\frac{\partial}{\partial r}\left(r\frac{\partial}{\partial r}\right)+\frac{1}{r^2}\frac{\partial^2}{\partial\phi^2}+\frac{\partial^2}{\partial z^2}-\frac{1}{c^2}\frac{\partial^2}{\partial t^2}\right]\Phi=0 \quad \text{(A2)}$$

where $r=\sqrt{x^2-y^2}$ represents a radial coordinate, ϕ is an azimuthal angle, z represents an axial axis that is perpendicular to the plane defined by r and ϕ, t is time and Φ represents acoustic pressure or Hertz potential that is a function of r, ϕ, z, and t.

Substituting (A1) into (A2), we have

$$\begin{aligned}&\left[\frac{1}{r}\frac{\partial}{\partial r}\left(r\frac{\partial}{\partial r}\right)+\frac{1}{r^2}\frac{\partial^2}{\partial\phi^2}+\frac{\partial^2}{\partial z^2}-\frac{1}{c^2}\frac{\partial^2}{\partial t^2}\right]\Phi_{J_m}\\&\quad=\cos m(\phi-\phi_0)e^{i(\beta z-\omega t)}\frac{1}{r}\frac{\partial}{\partial r}\left(r\frac{\partial J_m(\alpha r)}{\partial r}\right)\\&\qquad+J_m(\alpha r)e^{i(\beta z-\omega t)}\frac{1}{r^2}\frac{\partial^2\cos m(\phi-\phi_0)}{\partial\phi^2}\\&\qquad+J_m(\alpha r)\cos m(\phi-\phi_0)\left(\frac{\partial^2}{\partial z^2}-\frac{1}{c^2}\frac{\partial^2}{\partial t^2}\right)e^{i(\beta z-\omega t)}\\&\quad=\left(\frac{m^2}{r^2}-\alpha^2\right)\Phi_{J_m}+\left(-\frac{m^2}{r^2}\right)\Phi_{J_m}\\&\qquad+\left(\frac{\omega^2}{c^2}-\beta^2\right)\Phi_{J_m}.\end{aligned} \quad \text{(A3)}$$

Since

$$\beta^2=\frac{\omega^2}{c^2}-\alpha^2 \quad \text{(A4)}$$

the right-hand side of (A3) is zero, i.e., (A1) is an exact solution of (A2). Similarly, one can prove (6) is also an exact solution of (A2).

VIII. Appendix B

Derivation of a formula for calculating the pulse-echo response of any-order Bessel beam or X wave from a point scatterer under the Fresnel approximation [29].

Suppose that a transducer has an aperture of a radius, a, located at $z=0$ (see Fig. 11), the wave field at a spatial point $\vec{r}_0=(x_0,y_0,z)$ can be calculated with the Rayleigh–Sommerfeld diffraction formula [29]

$$\begin{aligned}\tilde{\Phi}(\vec{r}_0,\omega)=&\frac{1}{i\lambda}\int_0^a\int_{-\pi}^{\pi}\tilde{\Phi}(\vec{r}_1,\omega)e^{ikr_{01}}\frac{z}{r_{01}^2}r_1dr_1d\phi_1\\&+\frac{1}{2\pi}\int_0^a\int_{-\pi}^{\pi}\tilde{\Phi}(\vec{r}_1,\omega)e^{ikr_{01}}\frac{z}{r_{01}^3}r_1dr_1d\phi\end{aligned} \quad \text{(B1)}$$

where the first and second terms represent high and low frequency contributions, respectively, $\tilde{\Phi}(\vec{r}_0,\omega)$ is the wave field at the spatial point $\vec{r}_0$ and is the Fourier transform of $\Phi(\vec{r}_0,t)$, $\tilde{\Phi}(\vec{r}_1,\omega)$ is the wave field at a point $\vec{r}_1=(x_1,y_1,0)$ (source point) on the surface of the transducer and is the Fourier transform of $\Phi(\vec{r}_1,t)$, $r_1=\sqrt{x_1^2+y_1^2}$, $\phi_1=\tan^{-1}(y_1/x_1)$, λ is the wavelength, and r_{01} is the distance between the field point $\vec{r}_0$ and the source point $\vec{r}_1$, which is given by

$$r_{01}=\sqrt{(x_0-x_1)^2+(y_0-y_1)^2+z^2}. \quad \text{(B2)}$$

If we study the field on the plane $y_0=0$, the distance between the source and field points will be simplified (for the Bessel beams and X waves, fields on different planes can be obtained by rotating the transducer, i.e., changing ϕ_0, see (5) and (6)). Substituting $x_1=r_1\cos\phi_1$ and $y_1=r_1\sin\phi_1$ into (B2), we have

$$r_{01}=\sqrt{x_0^2+z^2}\sqrt{1+\frac{r_1^2-2x_0r_1\cos\phi_1}{x_0^2+z^2}}. \quad \text{(B3)}$$

With the Fresnel approximation (where r_1 and $x_0\ll\sqrt{x_0^2+z^2}$ and this condition is satisfied in our simulations), r_{01} in the denominators and phase terms of (B1) can be approximated by

$$r_{01}\approx\sqrt{x_0^2+z^2} \quad \text{(B4)}$$

and

$$r_{01}\approx\sqrt{x_0^2+z^2}+\frac{r_1^2}{2\sqrt{x_0^2+z^2}}-\frac{x_0r_1\cos\phi_1}{\sqrt{x_0^2+z^2}} \quad \text{(B5)}$$

respectively. Substituting (B4) and (B5) into (B1), one obtains

$$\begin{aligned}\tilde{\Phi}(\vec{r}_0,\omega)=&\left(\frac{1}{i\lambda}+\frac{1}{2\pi\sqrt{x_0^2+z^2}}\right)\frac{ze^{ik\sqrt{x_0^2+z^2}}}{(x_0^2+z^2)}\\&\cdot\int_0^a\tilde{\Phi}_1(r_1,\omega)e^{ik(r_1^2/2\sqrt{x_0^2+z^2})}\\&\cdot\left[\int_{-\pi}^{\pi}e^{-ik(x_0r_1/\sqrt{x_0^2+z^2})\cos\phi_1}\right.\\&\left.\cdot\cos m(\phi_1-\phi_0)d\phi_1\right]r_1dr_1\end{aligned} \quad \text{(B6)}$$

where $\tilde{\Phi}(\vec{r}_1,\omega)=\tilde{\Phi}_1(r_1,\omega)\cos m(\phi_1-\phi_0)$ (see (5) and (6)). Since [31]

$$J_m(z)=\frac{e^{-im\pi/2}}{2\pi}\int_{-\pi}^{\pi}e^{iz\cos\phi}\cos m\phi d\phi \quad \text{(B7)}$$

(B6) can be rewritten as (note that $\cos m(\phi_1-\phi_0)=\cos m\phi_1\cos m\phi_0+\sin\phi_1\sin\phi_0$ and integration of an odd function from $-\pi$ to π is zero)

$$\begin{aligned}\tilde{\Phi}(\vec{r}_0,\omega)=&\left(\frac{2\pi}{i\lambda}+\frac{1}{\sqrt{x_0^2+z^2}}\right)\frac{ze^{i(k\sqrt{x_0^2+z^2}+m\pi/2)}}{(x_0^2+z^2)}\\&\cdot\cos m\phi_0\int_0^a\tilde{\Phi}_1(r_1,\omega)e^{ik(r_1^2/2\sqrt{x_0^2+z^2})}\\&\cdot J_m\left(-k\frac{x_0r_1}{\sqrt{x_0^2+z^2}}\right)r_1dr_1\end{aligned} \quad \text{(B8)}$$

where

$$\tilde{\Phi}_1(r_1,\omega)=2\pi T(\omega)J_m(\alpha r_1) \quad \text{(B9)}$$

for Bessel beams (see (5)), and

$$\tilde{\Phi}_1(r_1,\omega)=\frac{2\pi}{c}B(k)J_m(kr_1\sin\zeta)H(k)e^{-a_0k} \quad \text{(B10)}$$

for X waves (see (25) in [20] or (6) in the text). Equation (B8) can be used for calculating any-order Bessel beams or X waves under the Fresnel approximation. It drops a double integration in (B1) to a single one, reducing the computation

COORDINATE SYSTEM FOR SIMULATION

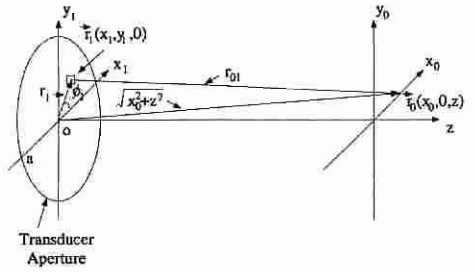

Fig. 11. Polar coordinate system for the derivation of a formula for calculating pulse-echo response of Bessel beams or X waves of any order under the Fresnel approximation. The wave sources and the receivers are located at $\vec{r}_1 = (x_1, y_1, 0)$, and the point scatterers are located at $\vec{r}_0 = (x_0, 0, z)$. The distance between $\vec{r}_0$ and $\vec{r}_1$ is r_{01}.

time significantly. From (B8), it is seen that the field of the limited diffraction beams at $\vec{r}_0$ changes as a cosine function, $\cos m\phi_0$, as the transducer rotates around its axis.

From the reciprocal principle and (B8), a formula for calculating the pulse-echo response of any-order Bessel beam or X wave for a point scatterer located at $\vec{r}_0$ (point spread function) under the Fresnel approximation can be obtained

$$e(\vec{r}_0, t) = \cos^2 m\phi_0 \mathcal{F}^{-1}\{\tilde{\Phi}_A^2(\vec{r}_0, \omega)\} \tag{B11}$$

where

$$\begin{aligned}\tilde{\Phi}_A(\vec{r}_0, \omega) = &\left(\frac{2\pi}{i\lambda} + \frac{1}{\sqrt{x_0^2 + z^2}}\right) \frac{z e^{i(k\sqrt{x_0^2+z^2} + m\pi/2)}}{(x_0^2 + z^2)} \\ &\cdot \int_0^a \tilde{\Phi}_1(r_1, \omega) e^{ik(r_1^2/2\sqrt{x_0^2+z^2})} \\ &\cdot J_m\left(-k\frac{x_0 r_1}{\sqrt{x_0^2 + z^2}}\right) r_1 dr_1 \end{aligned} \tag{B12}$$

and where $\mathcal{F}^{-1}$ is the inverse Fourier transform with respect to ω.

From (B11), the envelope of the point spread function of a limited diffraction pulse-echo system after the summation-subtraction of A-lines is given by

$$\begin{aligned}&|e_0(\vec{r}_0, t) - [e_2(\vec{r}_0, t)|_{\phi_0=0} + e_2(\vec{r}_0, t)|_{\phi_0=\pi/4}]| \\ &\quad = |\mathcal{F}^{-1}\{\tilde{\Phi}_{A0}^2(\vec{r}_0, \omega) - \tilde{\Phi}_{A2}^2(\vec{r}_0, \omega)\}|\end{aligned} \tag{B13}$$

where $\tilde{\Phi}_{A0}(\vec{r}_0, \omega) = \tilde{\Phi}_A(\vec{r}_0, \omega)|_{m=0}$ and $\tilde{\Phi}_{A2}(\vec{r}_0, \omega) = \tilde{\Phi}_A(\vec{r}_0, \omega)|_{m=2}$. This means that the sidelobes of the limited diffraction pulse-echo systems can be reduced with the summation–subtraction method if

$$\tilde{\Phi}_{A2}^2(\vec{r}_0, \omega) \approx \begin{cases} 0, & \vec{r}_0 \in \text{mainlobe} \\ \tilde{\Phi}_{A0}^2(\vec{r}_0, \omega), & \vec{r}_0 \in \text{sidelobes.} \end{cases}$$

ACKNOWLEDGMENT

The authors appreciate the secretarial assistance of Elaine C. Quarve and the graphic assistance of Julie M. Patterson.

REFERENCES

[1] J. N. Brittingham, "Focus wave modes in homogeneous Maxwell's equations: Transverse electric mode," *J. Appl. Phys.*, vol. 54, no. 3, pp. 1179–1189, 1983.
[2] R. W. Ziolkowski, "Exact solutions of the wave equation with complex source locations," *J. Math. Phys.*, vol. 26, no. 4, pp. 861–863, Apr. 1985.
[3] R. W. Ziolkowski, D. K. Lewis, and B. D. Cook, "Evidence of localized wave transmission," *Phys. Rev. Lett.*, vol. 62, no. 2, pp. 147–150, Jan. 9, 1989.
[4] J. Durnin, "Exact solutions for nondiffracting beams. I. The scalar theory," *J. Opt. Soc. Amer.*, vol. 4, no. 4, pp. 651–654, 1987.
[5] J. Durnin, J. J. Miceli, Jr., and J. H. Eberly, "Diffraction-free beams," *Phys. Rev. Lett.*, vol. 58, no. 15, pp. 1499–1501, Apr. 1987.
[6] K. Uehara and H. Kikuchi, "Generation of near diffraction-free laser beams," *Appl. Phys. B*, vol. 48, pp. 125–129, 1989.
[7] A. Vasara, J. Turunen, and A. T. Friberg, "Realization of general nondiffracting beams with computer-generated holograms," *J. Opt. Soc. Amer. A*, vol. 6, no. 11, pp. 1748–1754, 1989.
[8] D. K. Hsu, F. J. Margetan, and D. O. Thompson, "Bessel beam ultrasonic transducer: Fabrication method and experimental results," *Appl. Phys. Lett.*, vol. 55, no. 20, pp. 2066–2068, Nov. 13, 1989.
[9] J. A. Campbell and S. Soloway, "Generation of a nondiffracting beam with frequency independent beam width," *J. Acoust. Soc. Amer.*, vol. 88, no. 5, pp. 2467–2477, Nov. 1990.
[10] J. Lu and J. F. Greenleaf, "Ultrasonic nondiffracting transducer for medical imaging," *IEEE Trans. Ultrason., Ferroelec., Freq. Contr.*, vol. 37, pp. 438–447, Sept. 1990.
[11] —— "Pulse-echo imaging using a nondiffracting beam transducer," *Ultrasound Med. Biol.*, vol. 17, no. 3, pp. 265–281, May, 1991.
[12] —— "Evaluation of a nondiffracting transducer for tissue characterization," in *IEEE 1990 Ultrason. Symp. Proc.*, vol. 2, pp. 795–798, 1990.
[13] —— "Producing deep depth of field and depth-independent resolution in NDE with limited diffraction beams," *Ultrason. Imaging*, vol. 15, no. 2, pp. 134–149, Apr. 1993.
[14] —— "Formation and propagation of limited diffraction beams," *Acoustic Imaging*, vol. 20, to be published.
[15] —— "Effect on J_0 nondiffracting beam of deleting central elements of J_0 annular array transducer," *Ultrason. Imaging*, vol. 13, no. 2, p. 203, Apr. 1991 (Abs.).
[16] —— "Simulation of imaging contrast of nondiffracting beam transducer," *J. Ultrasound Med.*, vol. 10, no. 3, (suppl.), p. S4, Mar. 1991 (Abs.).
[17] —— "Experiment of imaging contrast of J_0 Bessel non-diffracting beam transducer," *J. Ultrasound Med.*, vol. 11, no. 3, (suppl.), p. S43, Mar. 1992 (Abs.).
[18] —— "Sidelobe reduction of nondiffracting pulse-echo images by deconvolution," *Ultrason. Imaging*, vol. 14, no. 2, p. 203, Apr. 1992 (Abs.).
[19] —— "New development in beam propagation," *J. Ultrasound Med.*, vol. 12, no. 3, (suppl.), p. S29, Mar. 1993 (Abs.).
[20] —— "Nondiffracting X waves—Exact solutions to free-space scalar wave equation and their finite aperture realizations," *IEEE Trans. Ultrason., Ferroelec., Freq. Cont.*, vol. 39, pp. 19–31, Jan. 1992.
[21] —— "Experimental verification of nondiffracting X waves," *IEEE Trans. Ultrason., Ferroelec., Freq. Cont.*, vol. 39, pp. 441–446, May 1992.
[22] J. Lu and J. F. Greenleaf, "Theory and acoustic experiments of nondiffracting X waves," *IEEE 1991 Ultrason. Symp. Proc.*, vol. 2, pp. 1155–1159, 1991.
[23] T. K. Song, J. Lu, and J. F. Greenleaf, "Modified X waves with improved field properties," *Ultrason. Imaging*, vol. 15, no. 1, pp. 36–47, Jan. 1993.
[24] J. Lu and J. F. Greenleaf, "Diffraction-limited beams and their applications for ultrasonic imaging and tissue characterization," in *Proc. SPIE New Developments in Ultrasonic Transducers and Transducer Systems*, vol. 1773, F. L. Lizzi, Ed., 1992, pp. 92–119.
[25] J. Lu, T. K. Song, R. R. Kinnick, and J. F. Greenleaf, " *In vitro* and *in vivo* real-time imaging with ultrasonic limited diffraction beams," *IEEE Trans. Med. Imaging*, vol. 12, Dec. 1993 (to be published).
[26] J. Lu and J. F. Greenleaf, "Steering of limited diffraction beams with a two-dimensional array transducer," in *IEEE 1992 Ultrason. Symp. Proc.* vol. 1, pp. 603–607, 1992.
[27] C. B. Burckhardt, P. A. Grandchamp, H. Hoffmann, "Methods for increasing the lateral resolution of B-scan," *Acoustic Holography*, vol. 5, 1973, pp. 391–413.
[28] M. S. Patterson, F. S. Foster, and D. Lee, "Sidelobes and speckle reduction for an eight sector conical scanner," in *IEEE 1981 Ultrason. Symp. Proc.*, vol. 2, pp. 632–637, 1981.

[29] J. W. Goodman, *Introduction to Fourier Optics*. New York: McGraw-Hill, 1968, chaps. 2–4.
[30] F. John, *Partial Differential Equations*. New York: Springer-Verlag, 1982.
[31] P. M. Morse and H. Feshbach, *Methods of Theoretical Physics*, Part I. New York: McGraw-Hill, 1953.
[32] R. Bracewell, *The Fourier transform and its Applications*. New York: McGraw-Hill, 1965, chaps. 4 and 6.
[33] A. V. Oppenheim and R. W. Schafer, *Digital Signal Processing*. Englewood Cliffs, NJ: Prentice-Hall, 1975, chap. 5.
[34] J. Lu and J. F. Greenleaf, "A study of sidelobe reduction for limited diffraction beams," in *IEEE 1993 Ultrason. Symp. Proc.*, 1993 to be published.
[35] B. D. Steinberg and Q. Zhu, "Measurement of resolution in the breast versus size of the imaging aperture," *J. Ultrasound Med.*, vol. 12, no. 3, (suppl.), p. S9, Mar. 1993 (Abs.).
[36] J. P. Wild, "A new method of image formation with annular apertures and application in radio astronomy," in *Proc. Royal Society, A*, vol. 286, pp. 499–509, 1965.
[37] M. S. Patterson and F. S. Foster, "Acoustic fields of conical radiators," *IEEE Trans. Sonics Ultrason.*, vol. SU–29, pp. 83–92, Mar. 1982.

Jian-yu Lu (M'88) was born in Fuzhou, Fujian Province, People's Republic of China, on August 20, 1959. He received the B.S. degree in electrical engineering in 1982 from Fudan University, Shanghai, China, the M.S. degree in 1985 from Tongji University, Shanghai, China, and Ph.D. degree in 1988 from Southeast University, Nanjing, China.

He is currently an Associate Consultant at the Biodynamics Research Unit, Department of Physiology and Biophysics, Mayo Clinic, Rochester, MN, and he is an Assistant Professor of Biophysics at the Mayo Medical School. From March 1990 to December 1991, he was a Research Associate at the Biodynamics Research Unit, and from December 1988 to February 1990, he was a Post-Doctoral Research Fellow there. Prior to that, he was a faculty member of the Department of Biomedical Engineering, Southeast University, Nanjing, China and worked with Prof. Yu Wei. His research interests are in acoustical imaging and tissue characterization, medical ultrasonic transducers, and ultrasonic beam propagation.

Dr. Lu is a recipient of the IEEE UFFC Outstanding Parer Award in the 1992 TRANSACTIONS. He is a member of the IEEE UFFC Society, American Institue of Ultrasound in Medicine, and Sigma Xi.

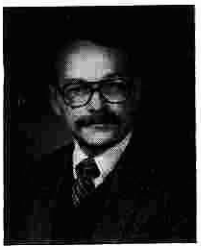

James F. Greenleaf (M'73–SM'84–F'88) was born in Salt Lake City, UT, on February 10, 1942. He received the B.S. degree in electrical engineering in 1964 from the University of Utah, Salt Lake City, the M.S. degree in engineering science in 1968 from Purdue University, Lafayette, IN, and the Ph.D. degree in engineering science from the Mayo Graduate School of Medicine, Rochester, MN, and Purdue University in 1970.

He is a Professor of Biophysics and Medicine, Mayo Medical School, and Consultant, Biodynamics Research Unit, Department of Physiology and Biophysics, and Cardiovascular Disease and Medicine, Mayo Foundation. His special field of interest is ultrasonic biomedical imaging science and has published more than 150 articles and edited four books.

Dr. Greenleaf has served on the IEEE Technical Committee of the Ultrasonics Symposium since 1985. He served on the IEEE-UFFC Subcommittee for the Ultrasonics in Medicine/IEEE Measurement Guide Editors, and on the IEEE Medical Ultrasound Committee. He is the President of the UFFC Society. He holds five patents and is the recipient of the 1986 J. Holmes Pioneer Award from the American Institute of Ultrasound in Medicine, a recipient of the IEEE UFFC Outstanding Parer Award in the 1992 TRANSACTIONS, and is a Fellow of the IEEE and the AIUM. He is the Distinguished Lecturer for the IEEE UFFC Society for 1990–1991.